JOURNAL OF AIRCRAFT
Vol. 44, No. 6, November–December 2007

Lift Enhancement by Static Extended Trailing Edge

Tianshu Liu,* J. Montefort,† W. Liou,‡ and S. R. Pantula§
Western Michigan University, Kalamazoo, Michigan 49008
and
Qamar A. Shams¶
NASA Langley Research Center, Hampton, Virginia 23681

DOI: 10.2514/1.31995

A static extended trailing edge attached to a NACA0012 airfoil section is studied for achieving lift enhancement at a small drag penalty. It is indicated that the thin extended trailing edge can enhance the lift, whereas the zero-lift drag is not significantly increased. Experiments and calculations are conducted to compare the aerodynamic characteristics of the extended trailing edge with those of the Gurney flap and the conventional flap. The extended trailing edge, as a simple mechanical device added on a wing without altering the basic configuration, has a good potential to improve the cruise flight efficiency.

Nomenclature

AR	=	wing aspect ratio
c	=	main airfoil chord
C_D	=	drag coefficient
C_{D0}	=	zero-lift drag coefficient
C_l	=	sectional lift coefficient
C_L	=	lift coefficient
C_{M_b}	=	bending moment
C_p	=	pressure coefficient
D	=	drag
D_E	=	plate flexural rigidity
e	=	Oswald's efficiency
E	=	Young's modulus
G_1	=	similarity parameter, $D_E/(l^3 q_\infty)$
h	=	Gurney flap height, plate thickness
l	=	static extended trailing-edge length
L	=	lift
q_∞	=	freestream dynamic pressure
Re_c	=	Reynolds number based on chord
U_∞	=	freestream velocity
w	=	plate deformation
x	=	chordwise coordinate
y	=	normal coordinate
α	=	angle of attack
$\gamma(x)$	=	vortex sheet strength
δ	=	deflection angle of the static extended trailing edge
ΔC_L	=	lift coefficient change
ΔC_D	=	drag coefficient change
ν	=	kinematical viscosity, Poisson's ratio
ρ_∞	=	freestream air density

Received 7 May 2007; revision received 14 August 2007; accepted for publication 17 August 2007. Copyright © 2007 by the American Institute of Aeronautics and Astronautics, Inc. All rights reserved. Copies of this paper may be made for personal or internal use, on condition that the copier pay the $10.00 per-copy fee to the Copyright Clearance Center, Inc., 222 Rosewood Drive, Danvers, MA 01923; include the code 0021-8669/07 $10.00 in correspondence with the CCC.

*Associate Professor, Department of Mechanical and Aeronautical Engineering, Parkview Campus; tianshu.liu@wmich.edu. Senior Member AIAA (Corresponding Author).

†Assistant Professor, Department of Mechanical and Aeronautical Engineering, Parkview Campus.

‡Professor, Department of Mechanical and Aeronautical Engineering, Parkview Campus.

§Graduate Student, Department of Mechanical and Aeronautical Engineering, Parkview Campus.

¶Scientist.

Introduction

IT HAS long been recognized that flaps can significantly alter wing aerodynamics for high-lift generation. Conventional flaps have larger drag; therefore, they are mainly deployed for takeoff and landing and are not suitable in cruise flight. Small trailing-edge devices such as Gurney flaps and divergent trailing edges for lift enhancement have attracted considerable attention in the aeronautical community. The Gurney flap was introduced by Liebeck [1] for aeronautical applications, and considerable measurements and calculations have been performed to determine the aerodynamic characteristics of wings with Gurney flaps at low speeds [2–9]. Measurements were also made at high speeds [10]. Gurney-flap-type tabs have been used along with vortex generators to enhance lift and suppress flow separation for a single-slotted-flap airfoil at large flap deflection [11]. Microflaps that can change the deflection angle were used for flutter suppression [12]. To mimic the behavior of bird feathers during landing, a self-adjusting movable flap close to the trailing edge was proposed by Bechert et al. [13], which was able to maintain higher lift when stall occurs. A review on trailing-edge devices and other control technologies is given by Stanewsky [14].

Measurements of avian wing geometry for extracting typical avian airfoil sections indicate that the merganser and owl wings have a very thin trailing edge that is a single layer of feathers extended from a "normal" airfoil section [15]. Naturally, a question is whether and how this unique trailing edge affects the global aerodynamic characteristics of the wing. This inspires the concept of a static extended trailing edge (SETE), as illustrated in Fig. 1a. The main airfoil element remains unchanged, but it is extended at the trailing edge by attaching a thin splitting plate of suitable length and rigidity. As shown in Fig. 1b, the basic geometrical parameters are the main airfoil chord c, length of the SETE l, and deflection angle δ. Depending on specific applications, the extension could be an aluminum plate, polymer membrane, composite sheet, or smart material plate. In general, a thin extended trailing edge is flexible such that it can be passively changed through flow–structure interaction or actively controlled by embedded actuators. In the current operating conditions, our analysis shows that when extended trailing edges are sufficiently rigid, their shapes are not sufficiently affected by flow and no vibration is induced. Thus, the cases studied here are static or quasi steady. The effects of SETE on the wing aerodynamics are mainly due to modifications of the airfoil camber and of the flow structure at the trailing edge. The lift enhancement by the SETE is, expectedly, due to the camber effect. It is speculated that the drag penalty of the SETE is small because it is usually embedded in the wake of the main airfoil. The drag penalty should be examined carefully in comparison with Gurney flaps and conventional flaps. The objective of this work is to study the SETE as an alternative flow

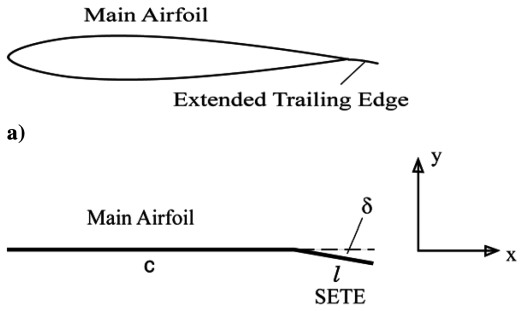

Fig. 1 Illustrations of a main airfoil a) with an extended trailing edge and b) geometrical parameters and coordinate system.

control technique for lift enhancement at a small drag penalty in cruise flight.

We first describe the geometrical features of the SETE and relevant similarity parameters. Experimental results are presented, including the lift and drag coefficients of the baseline NACA0012 airfoil model and of models with the SETE and Gurney flaps. The lift enhancement is achieved by the SETE, whereas the drag polar and lift-to-drag ratio remains largely unchanged. The zero-lift drag and Oswald's efficiency are not significantly affected by the SETE. The benefit analysis for the SETE in cruise flight is given in comparison with Gurney flap. Based on thin-airfoil theory and computational fluid dynamics (CFD) simulations, the aerodynamic characteristics of the SETE are further compared with those of the corresponding Gurney flap and conventional flap.

Wind Tunnel and Model

Tests were conducted in the Advanced Design Wind Tunnel (ADWT) at Western Michigan University. The ADWT is a low-speed, closed-circuit, single-return atmospheric tunnel with a test section that is 32 in. high, 45 in. wide, and 8 ft long. Full-test-section-length Plexiglas windows on the sides and ceiling allow optical access. The 161-ft-long circuit consists of two legs that are 65.6 ft long and the other two legs are 14.9 ft long. Low turbulence and good flow direction control are obtained by a combination of features, including four screens and a honeycomb in the stilling chamber, a 10:1 contraction ratio between the stilling chamber and test section, empirically tailored test section walls, tangential flow breathing at the test section exit to the diffuser, and a 5.4-deg diffuser angle. Under the present test conditions at $Re_c = 4.74 \times 10^5$, natural boundary-layer transition was observed at about 30% c on the NACA0012 airfoil model at a zero angle of attack (AOA) based on global luminescent-oil-film skin friction measurements [16]. The main drive power source is a 125-hp dc motor with a solid-state speed controller. The 16-blade fan is 6 ft in diameter. The flow velocity range is approximately 20 to 240 ft/s (6 to 73 m/s), in which the total temperature is in the range of 60 to 120°F. This corresponds to the dynamic pressures up to 65 lb/ft^2 and Reynolds numbers up to 1.3×10^6 per foot.

A six-component internal force balance (AeroLab) is installed in the ADWT. The balance measurement ranges are ±150 lb for lift, ±100 lb for side force, ±25 lb for axial force, ±250 in · lb for pitching moment, ±180 in · lb for yawing moment, and ±200 in · lb for rolling moment. A parallelogram linkage sting support system is able to set the angle of attack from −36 to 36 deg within the accuracy of 0.1 deg. A traverse system of two degrees of freedom is equipped for probes.

A ceramic NACA0012 airfoil section model was used in experiments. The chord and span of the model were 10 and 12 in., respectively. Along the wing span, two 1.875-in.-long and 6-in.-wide parts made of polycarbonate can be mounted to the baseline model with four screws for clamping the SETE at the trailing edge, and they can be easily removed to place different extended trailing edges. Several pieces of the SETE with different lengths were prepared for the tests, which were made of either aluminum or Mylar (PET polyester). Young's modulus and Poisson's ratio for aluminum were 70 GPa and 0.35, respectively, and Young's modulus and Poisson's ratio for Mylar were 2.8 GPa and 0.37, respectively. Figure 2 shows the NACA0012 airfoil model attached with a Mylar SETE and the model parts before assembly, including the baseline NACA0012 model, two removable parts for clamping the SETE, and typical aluminum SETE and Mylar SETE. To support the model, the end plates (18 by 13 in.) were mounted to the sting balance through two aluminum bars placed in a mounting bracket. The end plates also reduced the three-dimensionality of flow. Figure 3 shows the model mounted on the balance for testing in the ADWT.

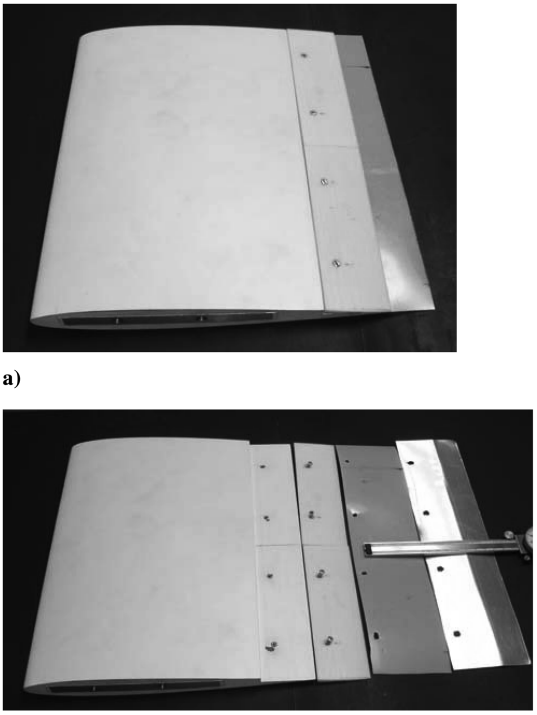

Fig. 2 Photographs of airfoil models: a) NACA0012 with a Mylar SETE and b) baseline model with removable parts and aluminum and Mylar SETEs.

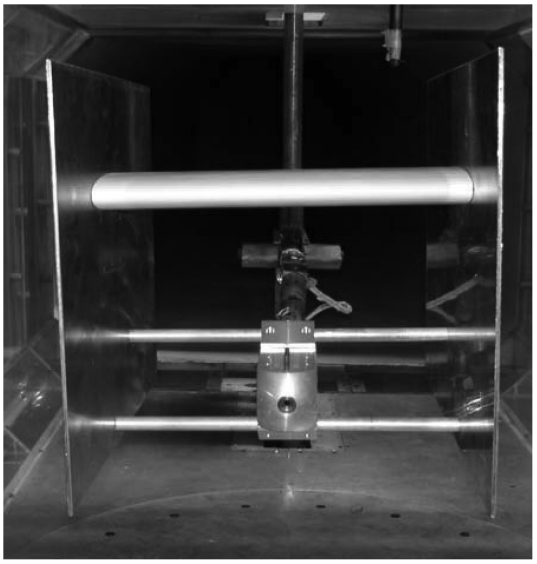

Fig. 3 NACA0012 airfoil model mounted on the end plates connected to a sting balance.

Similarity Parameters

The similarity parameters for a rigid airfoil with an extended trailing edge are considered. The similarity parameters for a rigid airfoil are Reynolds number $Re_c = U_\infty c/\nu$ and Mach number M_∞, where U_∞ is the freestream velocity and c is the airfoil chord. Because an extended trailing edge is attached to the rigid airfoil, additional similarity parameters should be obtained for achieving the complete flow and structure similarity. An extended trailing edge is generally considered to be flexible as a thin cantilever plate deforming under aerodynamic loading. The differential equation for the time-independent displacement w of a thin plate is generally expressed by $L[w(x, y)] = F(x, y)$ [17], in which x and y are the chordwise and normal coordinates, respectively; L is a linear differential operator; and $F(x, y)$ is an external distributed force on the plate. In our case, $F(x, y) = \Delta p$ is the aerodynamic pressure difference across the plate or aerodynamic load. For a homogenous plate, the operator $L = D_E\nabla^4$ is the biharmonic operator, in which $D_E = Eh^3/12(1 - \nu^2)$ is the plate flexural rigidity. The rigidity D_E depends on the plate thickness h, Young's modulus E, and Poisson's ratio ν.

Let us introduce the nondimensional variables $\bar{F} = F/q_\infty$, $\bar{w} = w/l$, $\bar{x} = x/l$, and $\bar{y} = y/l$, where $q_\infty = \rho_\infty U_\infty^2/2$ is the dynamic pressure and l is the length of the SETE. Thus, we have the nondimensional equation $G_1\nabla^4\bar{w} = \bar{F}$, where the main similarity parameter for aeroelasticity is $G_1 = D_E/(l^3 q_\infty)$. The functional relations for the lift and drag coefficients are $C_L = f_1(\alpha, Re_c, M_\infty, G_1, \delta, l/c)$ and $C_D = f_2(\alpha, Re_c, M_\infty, G_1, \delta, l/c)$. For the SETE, the similarity parameter G_1 should be sufficiently large such that the shape of the SETE is not changed significantly by flow. For the present low-speed experiments, M_∞ is very small and Re_c is fixed at 4.74×10^5. Although the effects of Re_c and M_∞ are worthwhile for further investigation, we mainly consider here the aerodynamic behavior of the NACA0012 airfoil model with the SETE in the parametric space (α, δ, and l/c).

Results and Discussions

Static Extended Trailing Edge

The lift and drag coefficients as a function of the AOA for the baseline NACA0012 airfoil model were measured at $Re_c = 4.74 \times 10^5$. According to McCormick's formula [18], the lift slope depends on the aspect ratio (AR) by

$$a = \frac{dC_L}{d\alpha} = \frac{a_0 AR}{AR + 2(AR + 4)/(AR + 2)} \quad (1)$$

where $a_0 = 2\pi$, according to thin-airfoil theory. A fit to the lift data of the baseline model using Eq. (1) gives the effective aspect ratio $AR = 4.42$ that is larger than the physical aspect ratio of 1.2. The end plates substantially reduced the three-dimensionality of flow. The drag coefficient is represented as a function of the lift coefficient squared and fitted using the classical relation $C_D = C_{D0} + C_L^2/\pi eAR$. Therefore, we obtain the zero-lift drag coefficient $C_{D0} = 0.014$ and the Oswald span efficiency $e = 0.8$ for the baseline model with $AR = 4.42$. Although the finite end plates do not completely eliminate the three-dimensionality of flow, they modify the tip vortices, acting like large winglets.

In tests, an aluminum sheet (0.216 mm thick) and a Mylar sheet (0.254 mm thick) were used as the SETE, for which the deflection angle was set a priori. The plate flexural rigidities of the aluminum sheet and Mylar sheet are $D_E = 0.067$ and 0.0044 Nm, respectively. Figure 4 shows the lift coefficient as a function of the AOA and drag polar for the model with the SETE at $Re_c = 4.74 \times 10^5$, where C_L and C_D are based on the projected wing area of the baseline model. The lengths of the SETE are 5 and 10% of the chord of the baseline model, and the preset deflection angles of the SETE are 0, 5, 7 and 10 deg. According to Fig. 4, the C_L distribution is shifted up and the lift is enhanced depending on the deflection angle and relative length of the SETE, whereas the drag polar basically remains unchanged. The drag polar curves are collapsed for different deflection angles, indicating that the zero-lift drag and Oswald's efficiency are not changed much. Stall occurs a few degrees earlier, particularly for larger deflections. For the model with zero deflection, C_L is almost the same as that of the baseline model when the AOA is less than 10 deg, but it is larger for higher AOA until stall. Typically, four and five repeated tests were conducted for each case, and the results were averaged. The measurement uncertainties in C_L are 0.001 for low AOA and 0.01 for high AOA. For C_D, the measurement errors are 0.0002 for low AOA and 0.003 for high AOA. In general, the lift and drag coefficients for the SETE are normalized based on the main airfoil chord rather than on the total projected chord that is a variable. For a direct comparison with other trailing-edge devices, both the main airfoil chord and total projected chord are used for normalization. It must be emphasized that the lift enhancement is mainly a result of an increase in the pressure difference across the main airfoil induced by the SETE due to the camber effect, and additional aerodynamic loading on the SETE itself is not significant.

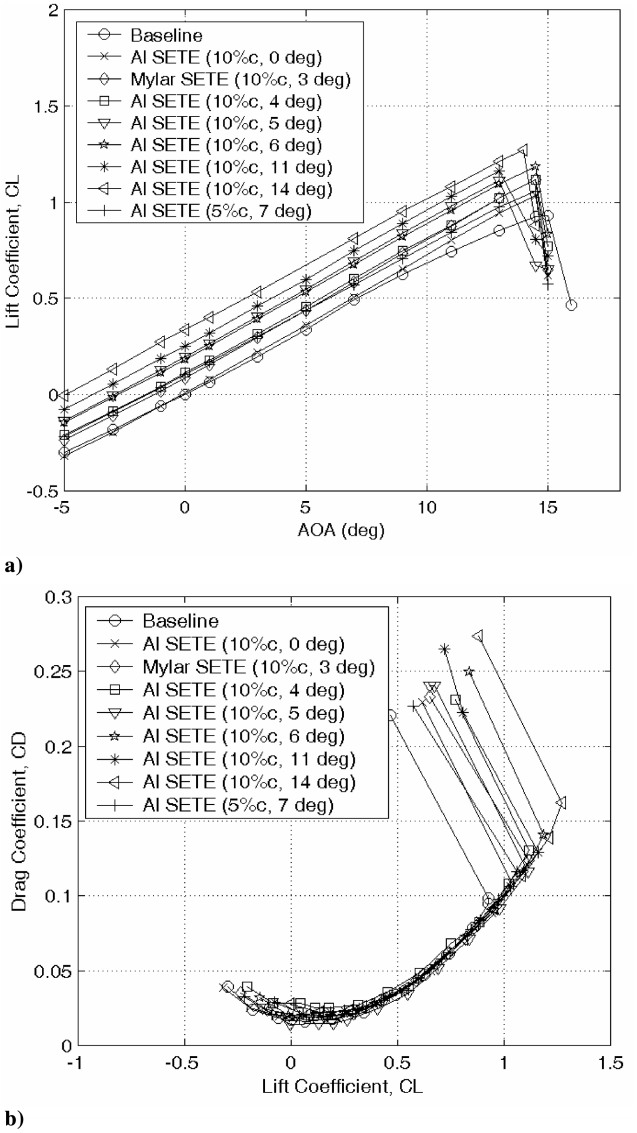

Fig. 4 NACA0012 airfoil model with the SETE at $Re_c = 4.74 \times 10^5$: a) lift coefficient as a function of the AOA and (b) drag polar.

Further, the drag coefficient is plotted as a function of the lift coefficient squared, as shown in Fig. 5a. All the data are basically collapsed into a single straight line, which is consistent with Fig. 4b. Both the zero-lift drag coefficient and Oswald's efficiency do not significantly change within the measurement accuracy for different deflection angles (small enough) and lengths of the SETE. It is indicated in Fig. 5a that the increased C_D results mainly from an increase of the induced drag $C_L^2/\pi eAR$ associated with the lift enhancement by the SETE. It is expected that this drag penalty will

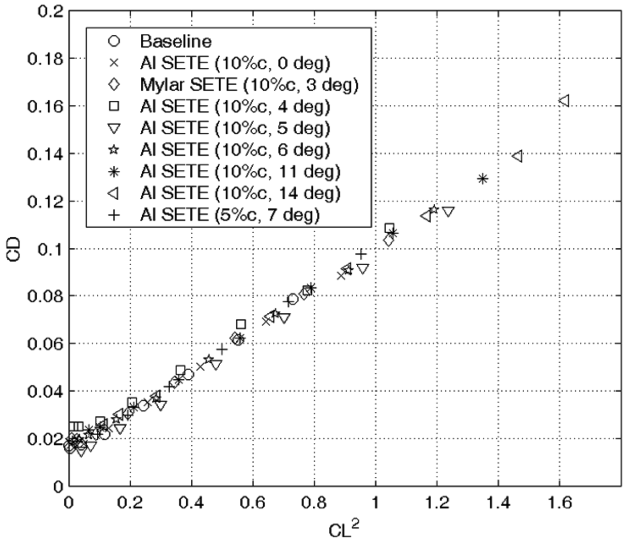

a)

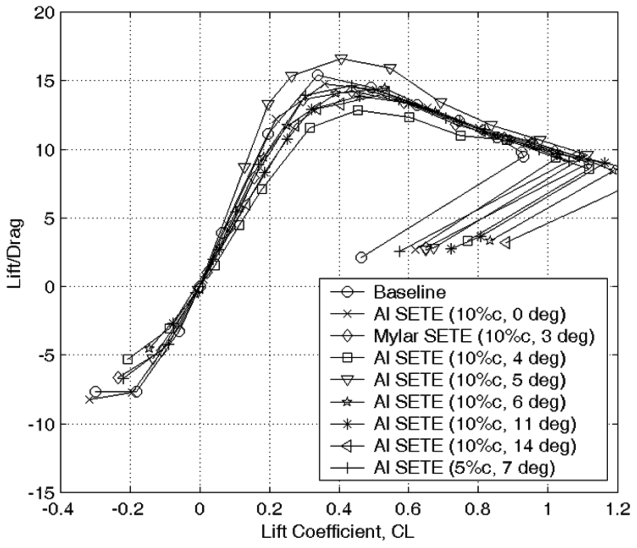

b)

Fig. 5 NACA0012 airfoil model with the SETE at $Re_c = 4.74 \times 10^5$: a) drag coefficient as a function of the lift coefficient squared and b) lift-to-drag ratio as a function of the lift coefficient.

be reduced as the aspect ratio increases. To examine the aerodynamic effectiveness of the SETE, the lift-to-drag ratio L/D is plotted in Fig. 5b as a function of C_L. The plots of L/D against C_L are approximately collapsed. However, the variations in L/D fail to show a systematical dependency on the deflection angle within $0.2 \leq C_L \leq 0.6$. Further investigation needs more precise and accurate measurements of drag. At this stage, a reasonable implication is that the SETE is able to increase C_L, whereas the variation in L/D is relatively small. The significance of these findings is that the SETE could improve the aerodynamic efficiency of cruise flight.

Comparison with Gurney Flaps

The aerodynamic characteristics of the SETE are compared with those of a Gurney flap, which is a short wall attached to the trailing edge that is perpendicular to the chord line on the pressure side of an airfoil, as illustrated in Fig. 6. Both the SETE and Gurney flap increase the lift at the cost of increasing the drag. However, there are some important quantitative differences between the SETE and Gurney flaps on the drag penalty. The measured results by Li et al. [7] for a NACA0012 rectangular wing indicate that L/D as a function of C_L for the wing with Gurney flaps (0.5–3%-c heights) is significantly lower than that for the baseline wing except at higher C_L. Unlike the

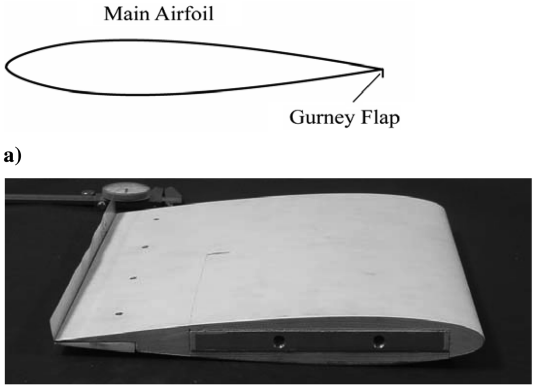

a)

b)

Fig. 6 Airfoil models with a Gurney flap: a) illustration of a main airfoil with a Gurney flap and b) photograph of NACA0012 with a Gurney flap.

SETE, the curves of L/D as a function of C_L for Gurney flaps do not collapse. Similar results can be found for other wings with Gurney flaps. The general conclusion is that Gurney flaps are not suitable for cruise flight due to the reduced L/D by the larger drag penalty. After fitting the data of Li et al. [7] using $C_D = C_{D0} + C_L^2/\pi eAR$, it is found that the zero-lift drag coefficient C_{D0} increases in a roughly linear fashion from 0.0065 for the baseline model to 0.021 for the 3%-c high Gurney flap, for which the effective aspect ratio is 46.5. The drag increase is caused by the extra form drag associated with open flow separation behind a Gurney flap.

To provide a direct comparison of the SETE with Gurney flaps, Gurney flap measurements were conducted using the same baseline NACA0012 airfoil model with the same chord Reynolds number. The Gurney flap height ranges from 1.2 to 6.75% c. Figure 6b shows the NACA0012 airfoil model with a Gurney flap. Figure 7 shows the lift coefficient as a function of the AOA and drag polar for the model with Gurney flaps at $Re_c = 4.74 \times 10^5$. The C_L curve is shifted up depending on the Gurney flap height, but C_D increases considerably except for the cases with 1.2 and 2.0% c. The drag coefficient is plotted as a function of the lift coefficient squared, as shown in Fig. 8a. The plots for the heights 1.2 and 2% c are close to that for the baseline model, whereas other curves are considerably shifted and the slope is also changed. This indicates that the zero-lift drag coefficient increases and Oswald's efficiency varies for Gurney flaps. These results are similar to the previously published data for a NACA0012 airfoil [7]. The lift-to-drag ratio is plotted in Fig. 8b as a function of C_L. Unlike the SETE, the L/D curves are not collapsed, and they are lower than the baseline data. Figure 9 shows a direct comparison between a 10%-c SETE with a 5-deg deflection angle and a 1.2%-c Gurney flap. The vertical displacement of the tip of the SETE is about 0.87% c, which is close to the Gurney flap height of 1.2% c. The lift enhancements in both cases are almost the same, but the Gurney flap suffers from a larger drag penalty, giving a smaller L/D than that for the SETE for all positive C_L.

To evaluate the net benefit of flow control in terms of the power required for cruise flight, Liu [19] proposed the following weight criterion:

$$\left[1 + \frac{6}{7}\left(\frac{\eta_{\mathrm{FC},r}}{b}\frac{C_L^{3/2}}{C_D}\right)W^{-1/6}\right]^{-1}\left(-\frac{6}{7}\frac{\Delta C_D}{C_D} + \frac{9}{7}\frac{\Delta C_L}{C_L}\right) - \frac{\Delta W}{W} > 0 \tag{2}$$

where $\Delta W/W$ is the ratio between the control system weight ΔW and the total aircraft weight W, and $\eta_{\mathrm{FC},r} = P_{\mathrm{FC},r}/\Delta W$ is the actuating power density. For an ideal weightless passive control device, the criterion is reduced to

$$-\frac{6}{7}\frac{\Delta C_D}{C_D} + \frac{9}{7}\frac{\Delta C_L}{C_L} = g > 0 \tag{3}$$

The function g is interpreted as a benefit margin for flow control. When g is positive, less engine power is required for cruise flight

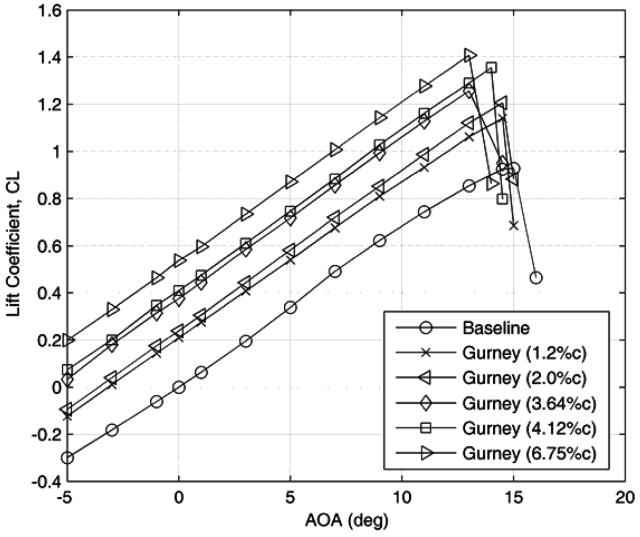

a)

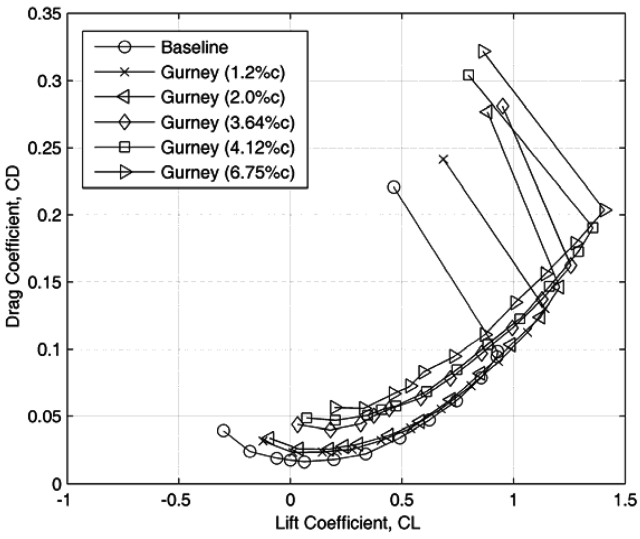

b)

Fig. 7 NACA0012 airfoil model with Gurney flaps at $Re_c = 4.74 \times 10^5$: a) lift coefficient and b) drag coefficient as a function of the AOA.

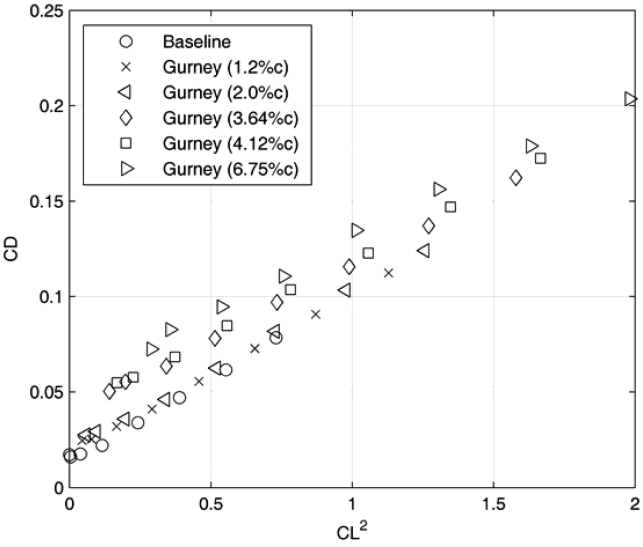

a)

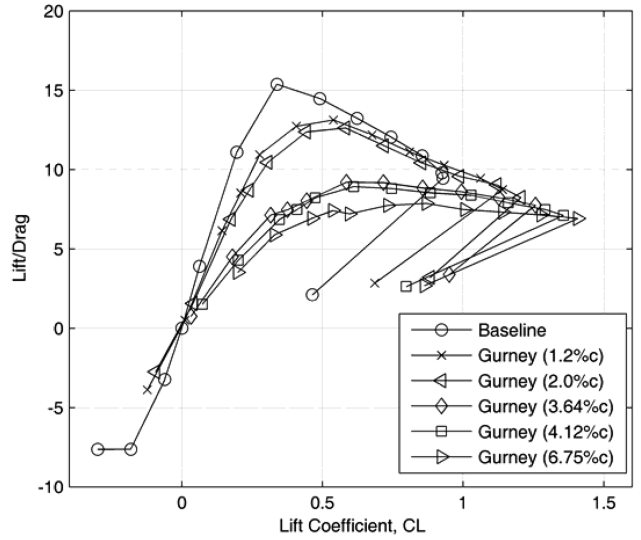

b)

Fig. 8 NACA0012 airfoil model with Gurney flaps at $Re_c = 4.74 \times 10^5$: a) drag coefficient as a function of the lift coefficient squared and b) lift-to-drag ratio as a function of the lift coefficient.

with passive flow control devices such as the SETE and Gurney flaps, and therefore the net benefit is achieved. Figure 10 shows the benefit margin for the SETE and Gurney flaps. For the SETE of the 10%-c length and deflection angle of 5 deg, its benefit margin remains positive and approaches zero as the AOA reaches 13 deg. This further confirms the feasibility of this SETE for improving the cruise flight efficiency. In contrast, for the 10%-c SETE with a deflection of 14 deg, the benefit margin becomes negative at about a 5-deg AOA. The Gurney flap with the 1.2%-c height has a similar behavior, whereas for the Gurney flap with the 4.12%-c height, g is considerably below zero after about a 3-deg AOA.

Thin-Airfoil Theory

Like conventional flaps, the lift enhancement by the SETE is generated by a change of the camber at the trailing edge. For geometrical simplicity, the main wing and SETE are modeled by straight segments, as shown in Fig. 1b. The total projected chord is $c' = c + l\cos\delta$. The slopes of the chord line segments are 0 for $0 \le x < c$ and $-\tan\delta$ for $c \le x < c'$. According to the classical thin-airfoil theory assuming that the slope is small [20], the strength of the vortex sheet is

$$\gamma(\theta) = 2U_\infty\left(A_0\frac{1+\cos\theta}{\sin\theta} + \sum_{n=1}^{\infty} A_n \sin n\theta\right) \tag{4}$$

where the angular variable is related the main chordwise coordinate by $x = (c'/2)(1-\cos\theta)$. The coefficients in Eq. (4) are $A_0 = \alpha + \tan\delta(1-\theta_c/\pi)$ and $A_n = (2/\pi n)\tan\delta\sin(n\theta_c)$ ($n = 1, 2, \ldots$). Here, the angular variable θ_c, which corresponds to the breaking point between the main wing and SETE, is given by $\theta_c = \cos^{-1}[(\varepsilon-1)/(\varepsilon+1)]$, where $\varepsilon = (l/c)\cos\delta$.

The sectional lift coefficient is given by

$$C_l = \frac{L'}{(1/2)\rho_\infty U_\infty^2 c} = 2\pi(1+\varepsilon)[\alpha + \tan\delta(1-\theta_c/\pi + \sin\theta_c/\pi)] \tag{5}$$

The positive deflection angle of the SETE shifts the C_l curve upward (lift enhancement) and slightly increases the lift slope. The moment coefficient around the one-fourth total chord is

$$C_{m,c'/4} = \frac{M'_{c'/4}}{(1/2)\rho_\infty U_\infty^2 c^2} = (1/4)(1+\varepsilon)^2\tan\delta(\sin 2\theta_c - 2\sin\theta_c) \tag{6}$$

where $C_{m,c'/4}$ is defined to be positive when it is the nose-up moment. Clearly, the positive deflection angle produces a negative moment. Furthermore, the pressure coefficient difference between the pressure and upper surfaces of the airfoil is $\Delta C_p = 2\gamma(x)/U_\infty$.

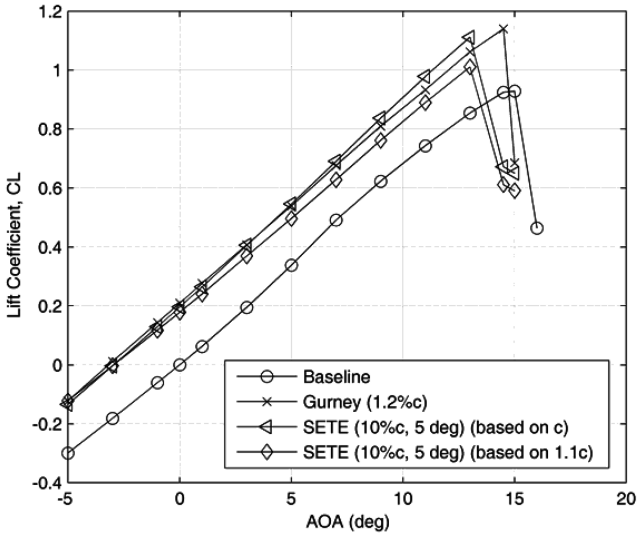

a)

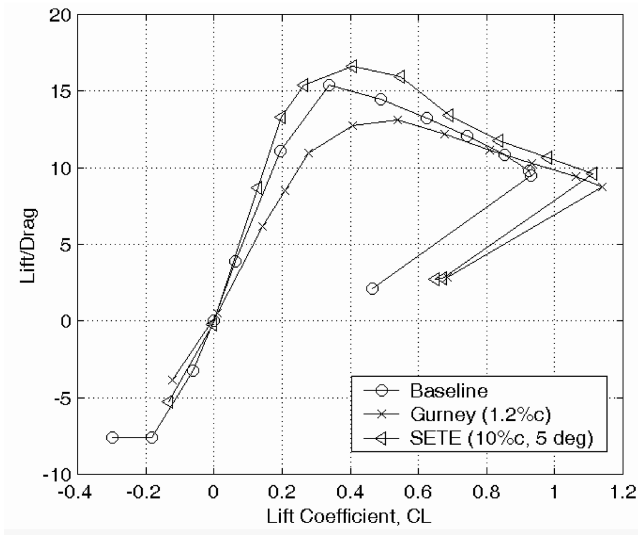

b)

Fig. 9 Comparison between the SETE and Gurney flap on the a) lift coefficient as a function of the AOA and the b) lift-to-drag ratio as a function of the lift coefficient for the NACA0012 airfoil model at $Re_c = 4.74 \times 10^5$.

For a finite rectangular wing, the effective angle of attack is $\alpha - (1+\tau)C_L/\pi AR$, where AR is the effective aspect ratio and the parameter τ is a function of $AR/2\pi$ for a rectangular wing [21]. A convenient regression formula is $\tau = -0.0476(AR/2\pi)^2 + 0.2195(AR/2\pi)$ for $AR/2\pi \in [0.25, 1.75]$. Hence, the lift enhancement $\Delta C_L = C_L - C_{L,\text{baseline}}$ for a finite rectangular wing can be calculated, where the lift coefficient for the wing with the SETE and baseline wing are, respectively,

$$C_L = \left[1 + \frac{2(1+\tau)}{AR}\right]^{-1} C_l \tag{7}$$

and

$$C_{L,\text{baseline}} = \left[1 + \frac{2(1+\tau)}{AR}\right]^{-1} 2\pi\alpha \tag{8}$$

According to the preceding relations, the lift enhancement by the SETE is

$$\Delta C_L = 2\left[1 + \frac{2(1+\tau)}{AR}\right]^{-1} [\pi\varepsilon\alpha + (1+\varepsilon)\tan\delta(\pi - \theta_c + \sin\theta_c)] \tag{9}$$

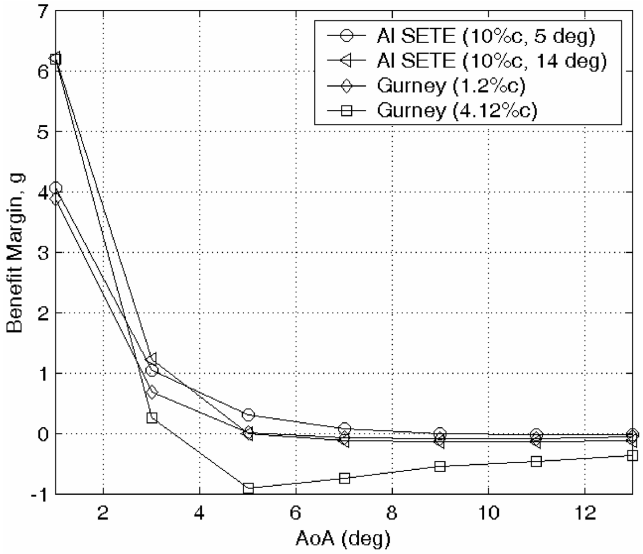

Fig. 10 Benefit margins of the SETE and Gurney flaps for cruise flight.

The difference of the pressure coefficient between the pressure and upper surfaces of the main wing is sensitively affected by the SETE. These results indicate a direct correlation of the aerodynamic loading between the main airfoil and the SETE. Figure 11 is a comparison between the predicted ΔC_L by thin-airfoil theory and the experimental and CFD data for the NACA0012 airfoil section ($AR = 4.42$ and $l/c = 0.1$) with the SETE. The near-linear relation given by thin-airfoil theory reasonably describes the initial trend of the experimental results for small deflections. However, the experimental data saturate as the deflection angle increases further, which may be caused by a reduced effective deflection due to the viscous effect. Two-dimensional CFD calculations using a Navier–Stokes code (Fluent), assuming that the boundary layer on the NACA0012 airfoil with the SETE is fully turbulent, predict the smaller lift enhancement.

Thin-airfoil theory has been expanded for the lift problem of an airfoil with a Gurney flap [22]. A solution of the generalized thin-airfoil integral equation for the vortex strength can be obtained by the method of successive approximations. The Gurney flap lift enhancement is interpreted as a special camber effect. The lift coefficient increment (pitching moment as well) is given as a square-root function of the relative Gurney flap height (i.e., $\Delta C_L \propto \sqrt{h/c}$). For comparison with the Gurney flap, the vertical displacement of the SETE is defined as $h/c = (l/c)\sin\delta$. Therefore, ΔC_L by the SETE

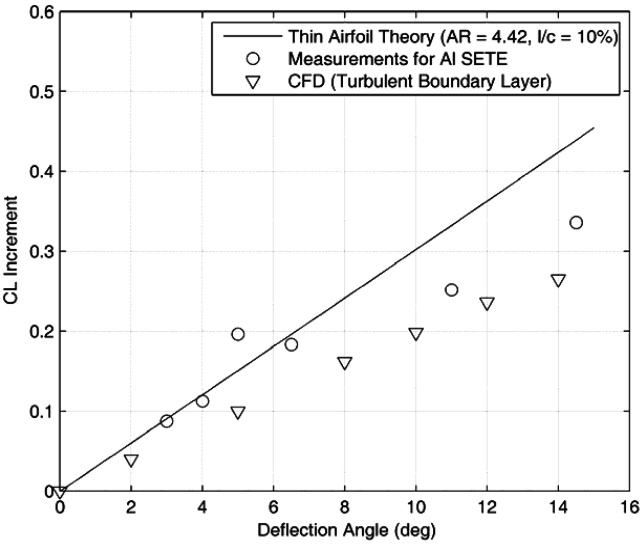

Fig. 11 Measured lift enhancement compared with thin-airfoil theory and CFD data for the NACA0012 airfoil model with the SETE.

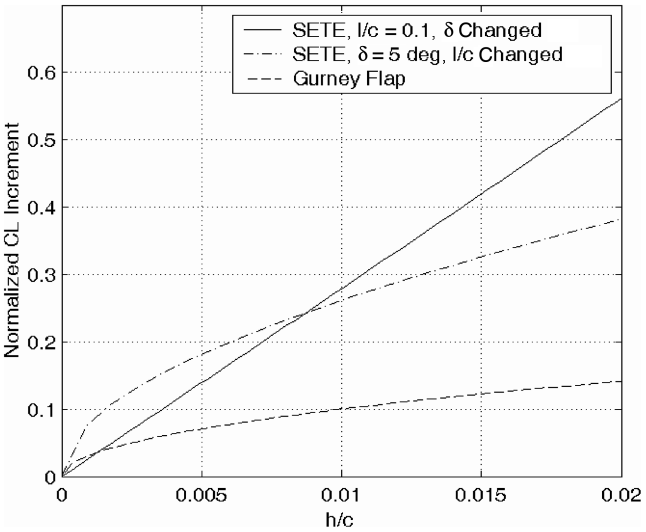

Fig. 12 Comparison of normalized lift enhancement between the SETE and Gurney flap based on thin-airfoil theory.

depends on the relative length l/c and deflection angle δ. Figure 12 shows the normalized ΔC_L as a function of h/c for the SETE and the Gurney flap according to thin-airfoil theory. Interestingly, ΔC_L increases in a linear fashion as an increase of the deflection angle for the SETE with a fixed length, whereas ΔC_L follows a square-root relation for both the Gurney flap and the SETE, with a variable length for a fixed deflection angle.

Deformation and Bending Moment

The aluminum and Mylar sheets as the SETE are usually set at nominal deflection angles in experiments, assuming they are sufficiently rigid. Nevertheless, small aeroelastic deformation relative to the neutral position always exists. To estimate the elastic deformation of the SETE, we consider a 2D clamped thin plate deformed due to aerodynamic load. The nondimensional deformation $\bar{w} = w/l$ is given by

$$\bar{w}(\bar{x}) = G_1^{-1} \int_0^{\bar{x}} \mathrm{d}\bar{x}_1 \int_0^{\bar{x}_1} \mathrm{d}\bar{x}_2 \int_0^{\bar{x}_3} \mathrm{d}\bar{x}_3 \int_0^{\bar{x}_3} \Delta C_p(\bar{x}_4)\, \mathrm{d}\bar{x}_4 + \frac{A\bar{x}^3}{6} + \frac{B\bar{x}^2}{2} \tag{10}$$

where $\bar{x} = x/l$ is the normalized chordwise coordinate from the breaking point between the main element and the SETE, $G_1 = D_E/(l^3 q_\infty)$, $A = 2G_1^{-1}(g_1 - g_2)$, $A = G_1^{-1}(g_2 - 2g_1)$, and

$$g_1 = \int_0^1 \mathrm{d}\bar{x}_1 \int_0^{\bar{x}_1} \mathrm{d}\bar{x}_2 \int_0^{\bar{x}_2} \Delta C_p(\bar{x}_3)\, \mathrm{d}\bar{x}_3$$

$$g_2 = \int_0^1 \mathrm{d}\bar{x}_1 \int_0^{\bar{x}_1} \Delta C_p(\bar{x}_2)\, \mathrm{d}\bar{x}_2$$

The pressure coefficient difference $\Delta C_p = 2\gamma(x)/U_\infty$ from thin-airfoil theory is substituted into Eq. (10) and numerical integration is carried out. The normalized deformation $\bar{w}/\sin\delta$ is calculated as a function of $\bar{x} = x/l$ for the 0.216-mm-thick aluminum sheet ($G_1 = 5.74$ and 10% c) and 0.254-mm-thick Mylar sheet ($G_1 = 0.38$ and 10% c). The deformation of the aluminum SETE is less than 1% of the vertical tip displacement $l \sin\delta$, whereas for the Mylar SETE it could be 13%. To estimate the actuating power required for deflecting the SETE, the bending moment relative to the breaking point between the main element and the SETE is estimated. The bending moment coefficient is defined as

$$C_{M_b} = \frac{M_b}{q_\infty l^2} = \int_0^1 \Delta C_p(\bar{x})\, \bar{x}\, \mathrm{d}\bar{x}$$

The bending moment coefficient is a linear function of the AOA for the SETE with a given deflection angle. The bending moment for the 2D case is on the order of $q_\infty l^2$.

CFD Simulations

To provide further insights to the lift enhancement by the SETE, the flow characteristics around a NACA0012 airfoil with the SETE were studied using CFD simulations at $Re_c = 4.74 \times 10^5$. The problem of a steady turbulent flow over the airfoil was solved using the commercial code Fluent on a C-grid. Grid independence was validated by comparing pressure distributions along the airfoil at two different angles of attack with published results [23]. The lift and drag coefficients were also compared with the published data [23]. The boundary layers were assumed to be fully turbulent, and the realizable k-ε turbulence model with the nonequilibrium wall function was used.

Figure 13 shows how the defection angle of the SETE affects the pressure coefficient distribution on the airfoil for a zero AOA. The aerodynamic loading on the SETE itself ($x/c > 1$) is not large, and the lift enhancement is mainly produced by the overall aerodynamic change on the main airfoil induced by the SETE. Comparisons of the calculated and measured lift coefficients are shown in Fig. 14 as a function of the AOA. The calculated results for the 2D airfoil are converted to the 3D wing results using Eq. (7). The calculated and experimental results are consistent until the calculated lift coefficients level at higher AOAs. As indicated in Fig. 11, the calculated increment in the lift coefficient exhibits the same trend as the experimental and theoretical results as a function of the deflection angle of the SETE. Figure 15 shows velocity magnitude contours around the NACA0012 airfoil with a zero AOA for 0- and 5-deg deflection angles. The asymmetry of the flowfield is induced by the deflected SETE and the wake is turned downward, indicating a deflected momentum stream tube and the generation of additional lift. The wake structure is not appreciably altered, although it is deflected; this implies that the parasite drag is not significantly affected.

Further, a 10%-c SETE with a 5-deg deflection angle is compared with a corresponding conventional plain flap that is simply a rear segment of a NACA0012 airfoil deflected at the 90% chord. Figure 16 shows the computed lift and drag coefficients as a function of the deflection angle for the SETE and plain flap. Compared with the plain flap, the lift enhancement by the SETE is larger, whereas the drag coefficient is smaller. Here, the lift and drag coefficients for the SETE are defined based on the main airfoil chord c. Even when these coefficients are based on 1.1 c for the SETE, the preceding results are still valid. The pressure coefficient distributions on the main airfoil for the SETE (5-deg deflection), plain flap (5-deg deflection), and

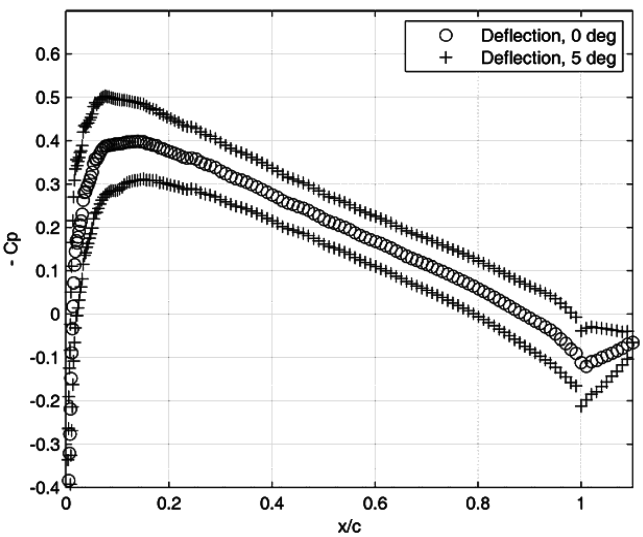

Fig. 13 Calculated pressure coefficient distributions on the NACA0012 airfoil for the SETE deflection angles of 0 and 5 deg at a zero AOA.

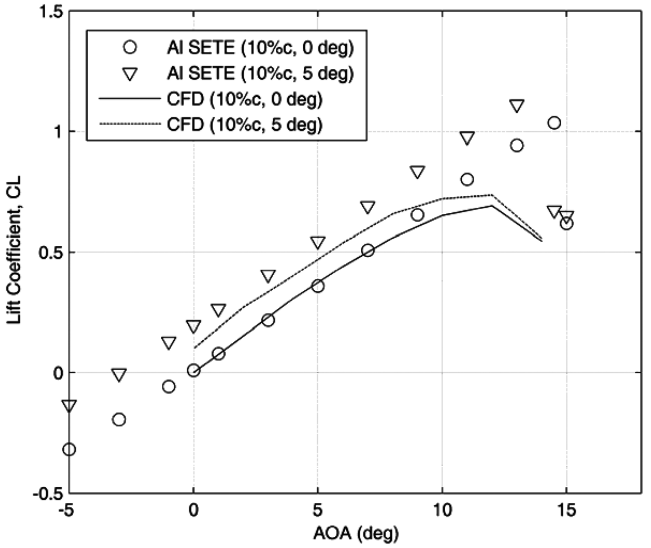

Fig. 14 Comparisons of the calculated and measured lift coefficients as a function of the AOA for the deflection angles of 0 and 5 deg.

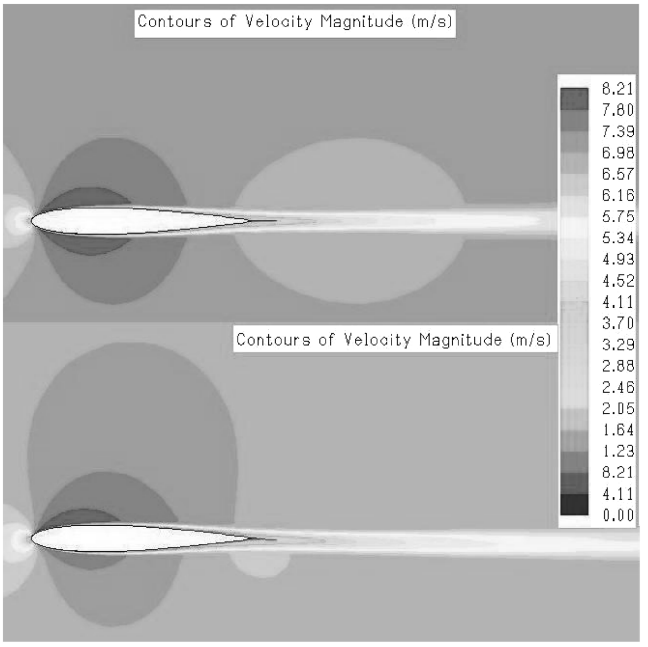

Fig. 15 Velocity magnitude fields of the NACA0012 airfoil for zero deflection of the SETE and 5 deg deflection of the SETE at a zero AOA.

Gurney flap are shown in Fig. 17, indicating that the larger pressure difference on the main airfoil is induced by the SETE. The Gurney flap height is $0.1\,c\,\sin(5\,\text{deg}) \approx 0.87\%\,c$, which is the same as the maximum vertical displacement of the SETE. Figures 18 and 19 show the lift coefficient as a function of the AOA and the drag polar for the SETE, plain flap, and Gurney flap. The lift and drag coefficients normalized by 1.1 c for the SETE are also shown in the figures for more reasonable comparison to eliminate the effect of the increased projected area. Among these trailing-edge devices, the SETE generates a large lift increase at a small drag penalty, and the lift enhancement is mainly produced by the camber effect rather than the increased area. It should be noted here that the absolute accuracy of the drag predicted by CFD is not critically examined, although the computed drag coefficient for the NACA0012 airfoil is close to $C_D = 0.02$–0.03, given by measurements for the corresponding airfoil section. Therefore, the preceding comparison in the drag polar is valid only in a relative sense. Furthermore, for the 2D airfoil, the drag polar is not parabolic because no induced drag is included.

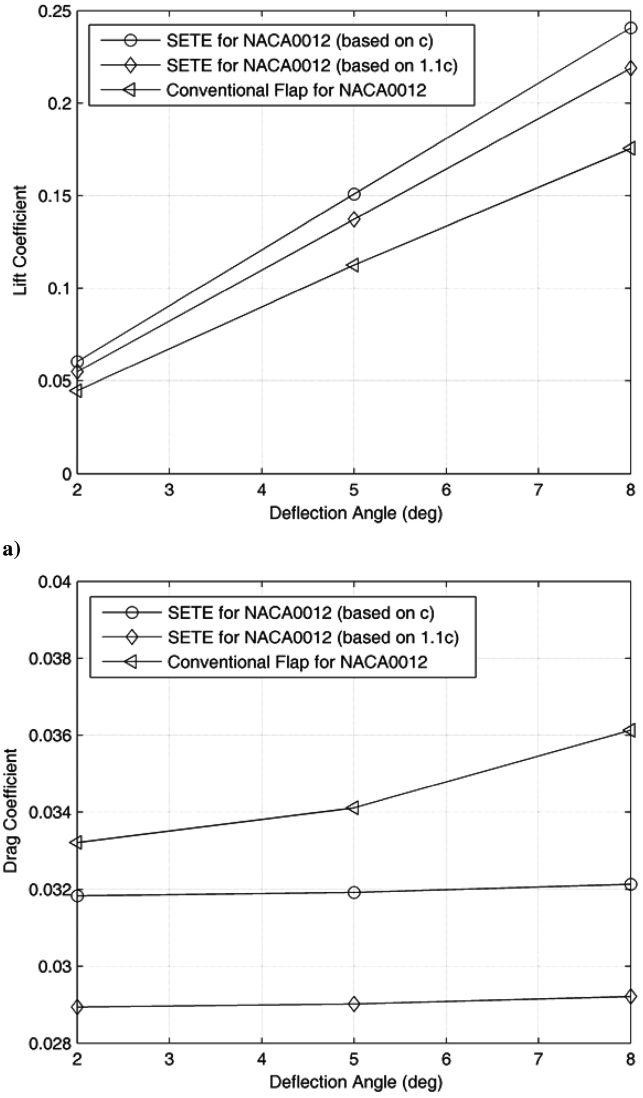

Fig. 16 Comparison of the computed lift and drag coefficients between the SETE and conventional flap for a NACA0012 airfoil at a zero AOA.

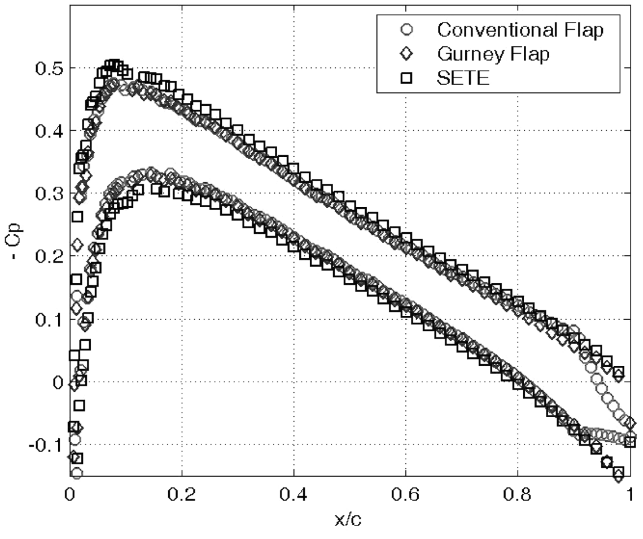

Fig. 17 Comparison of the computed pressure coefficient between the SETE, conventional flap and Gurney flap for a NACA0012 airfoil at a zero AOA.

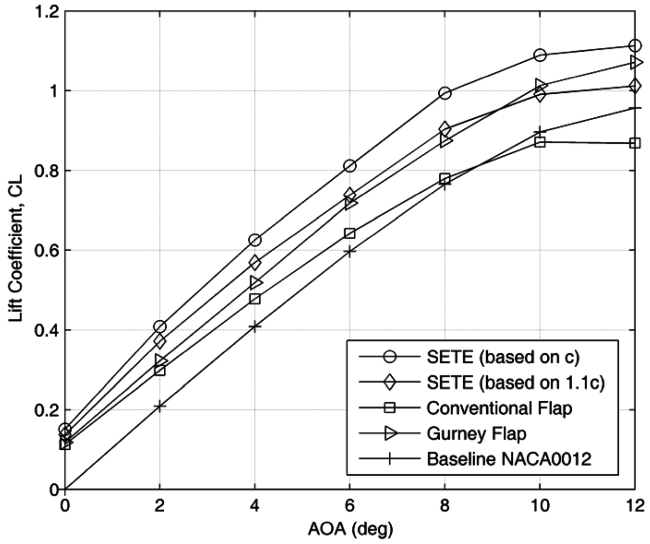

Fig. 18 Computed lift coefficient as a function AOA for the SETE (5-deg deflection), Gurney flap and conventional flap (5-deg deflection) for a NACA0012 airfoil.

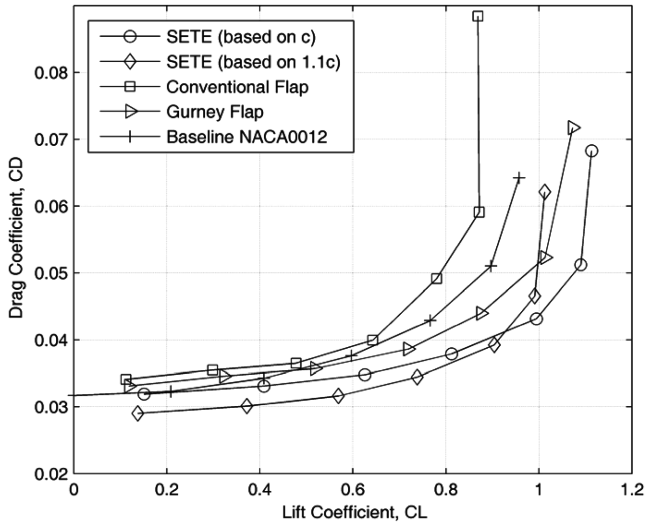

Fig. 19 Computed drag polar for the SETE (5-deg deflection), Gurney flap and conventional flap (5-deg deflection) for a NACA0012 airfoil.

Conclusions

Experiments and calculations presented show that a static extended trailing edge (SETE) attached to a NACA0012 airfoil model is able to enhance the lift, whereas the zero-lift drag is not significantly increased. The lift enhancement mechanism by the SETE is the camber effect, which is the same as that for other high-lift devices such as a Gurney flap and conventional flap. However, compared with a Gurney flap and conventional flap, the SETE generates a larger lift increase at a smaller drag penalty because it is embedded in the wake of the main airfoil. Therefore, the SETE has a promising potential for improving the cruise flight efficiency. The benefit margin of the SETE for cruise flight is evaluated in comparison with the Gurney flap, and the feasibility of the SETE for lift enhancement in cruise flight is demonstrated at small angles of attack and deflection angles of the SETE. The mechanical simplicity of the SETE allows direct application to aircraft without changing the basic aerodynamic configuration. Furthermore, the deformation and pitching moment of the SETE due to aerodynamic loading are estimated, and actuating the SETE is feasible because the pitching moment on it is small. Future research will focus on the SETE actuation using smart materials such as piezoactuators and shape memory alloys for steady and unsteady flow control.

Acknowledgment

This work was supported by the U.S. Air Force Office of Scientific Research under grant number FA9550-06-1-0187.

References

[1] Liebeck, R. H., "Design of Subsonic Airfoils for High Lift," *Journal of Aircraft*, Vol. 15, No. 9, 1978, pp. 547–561.

[2] Storms, B., and Jang, C. S., "Lift Enhancement of an Airfoil Using a Gurney Flap and Vortex Generators," *Journal of Aircraft*, Vol. 31, No. 3, 1994, pp. 542–547.

[3] Ross, J., Storms, B. L., and Carrannanto, P. G., "Lift-Enhancing Tabs on Multielement Airfoils," *Journal of Aircraft*, Vol. 32, No. 3, 1995, pp. 649–655.

[4] Myose, R., Papadakis, M., and Heron, I., "Gurney Flap Experiments on Airfoils, Wings, and Reflection Plane Model," *Journal of Aircraft*, Vol. 35, No. 2, 1998, pp. 206–211.

[5] Jang, C. S., Ross, J. C., and Cummings, R. M., "Numerical Investigation of an Airfoil with a Gurney Flap," *Aircraft Design*, Vol. 1, No. 2, 1998, pp. 75–88. doi:10.1016/S1369-8869(98)00010-X

[6] Jeffrey, D., Zhang, X., and Hurst, D. W., "Aerodynamics of Gurney Flaps on a Single-Element High-Lift Wing," *Journal of Aircraft*, Vol. 37, No. 2, 2000, pp. 295–301.

[7] Li, Y., Wang, J., and Zhang, P., "Effects of Gurney Flaps on a NACA0012 Airfoil," *Flow, Turbulence and Combustion*, Vol. 68, No. 1, 2002, pp. 27–39. doi:10.1023/A:1015679408150

[8] Gai, S. L., and Palfrey, R., "Influence of Trailing-Edge Flow Control on Airfoil Performance," *Journal of Aircraft*, Vol. 40, No. 2, 2003, pp. 332–337.

[9] Meyer, R., Hage, W., Bechert, D. W., Schatz, M., and Thiele, F., "Drag Reduction on Gurney Flaps by Three-Dimensional Modification," *Journal of Aircraft*, Vol. 43, No. 1, 2006, pp. 132–140.

[10] Bechert, D. W., Stanewsky, E., and Hage, W., "Wind Tunnel Measurements on a Transonic Wing with Flow Control by Various Devices," DLR, German Aerospace Research Center Rept. DLR-IB 223-99C05/IB 92517-99/b3-2, Stuttgart, Germany, June 1999.

[11] Storms, B., and Ross, J., "Experimental Study of Lift-Enhancement Tabs on a Two-Element Airfoil," *Journal of Aircraft*, Vol. 32, No. 5, 1995, pp. 1072–1078.

[12] Lee, H. T., Kroo, I. M., and Bieniawski, S., "Flutter Suppression for High Aspect Ratio Flexible Wings Using Microflaps," AIAA Paper 2002-1717 22–25 Apr. 2002.

[13] Bechert, D. W., Bruse, M., Hage, W., and Meyer, R., "Biological Surfaces and their Technological Applications—Laboratory and Flight Experiments on Drag Reduction and Separation Control," AIAA Paper 97-1960, June 1997.

[14] Stanewsky, E., "Adaptive Wing and Flow Control Technology," *Progress in Aerospace Sciences*, Vol. 37, No. 7, 2001, pp. 583–667. doi:10.1016/S0376-0421(01)00017-3

[15] Liu, T., Kuykendoll, K., Rhew, R., and Jones, S., "Avian Wing Geometry and Kinematics," *AIAA Journal*, Vol. 44, No. 5, 2006, pp. 954–963.

[16] Liu, T., Montefort, J., Woodiga, S., Merati, P., and Shen, L., "Global Luminescent Oil Film Skin Friction Meter," *AIAA Journal*, 2007 (to be published).

[17] Meirovitch, L., *Analytical Methods in Vibrations*, Macmillan, New York, 1967, Chap. 7.

[18] McCormick, B. W., *Aerodynamics, Aeronautics, and Flight Mechanics*, 2nd ed., Wiley, New York, 1995, p. 116.

[19] Liu, T., "Weight Criterion on Flow Control in Flight," *Journal of Aircraft*, Vol. 44, No. 1, 2007, pp. 348–351. doi:10.2514/1.28188

[20] Anderson, J. D., *Fundamentals of Aerodynamics*, 2nd ed., McGraw–Hill, New York, 1984, Chap. 4.

[21] Glauert, H., *The Element of Aerofoil and Airscrew Theory*, 2nd ed., Cambridge Univ. Press, Cambridge, England, U.K., 1999, Chap. 11.

[22] Liu, T., and Montefort, J., "Thin-Airfoil-Theoretical Interpretation for Gurney Flap Lift Enhancement," *Journal of Aircraft*, Vol. 44, No. 2, 2007, pp. 667–671. doi:10.2514/1.27680

[23] Hegna, H. A., "A Numerical Solution of Incompressible Turbulent Flow over Airfoils," AIAA Paper 1981-47, 12–15 Jan. 1981.